

Aerosol as a climate-forming component of the atmosphere.

2. Direct and indirect impact on climate

K.Ya. Kondratyev

Center for Ecological Safety RAS/Nansen Environmental and Remote Sensing Center, St. Petersburg

Received October 5, 2001

Atmospheric aerosol as a climate-forming agent of the atmosphere is studied with emphasis on sulfate aerosol, as well as on the problem of cloud–aerosol interaction (indirect aerosol impact on climate). It is shown that the problem of assessing the aerosol impact on climate is still far from complete solution. In this regard, some prospects for future research are suggested.

Introduction

Despite being not new, the problem of climate impact of atmospheric aerosol^{1–78} has received a definitely increased attention recently due to the need in reliable estimates of aerosol (primarily anthropogenic aerosol) impact on global climate. The Intergovernmental Panel on Climate Change (IPCC)-2001 Report clearly reflects this situation.¹⁵ In the first part of that review,³⁵ the physical properties and chemical composition of aerosol are quite extensively discussed.

As was already noted earlier, the IPCC-2001 Report undoubtedly provides voluminous, though not all, important information. Paradoxically, this international publication, although claimed as highly objective and all-inclusive, does not include even references to important results published (in particular, in English) by Russian specialists (probably, because there was no one scientist from Russia in the corresponding IPCC workgroups). It should be noted that only ten of many references included in this review are reproduced from Chapter 5 (devoted to direct and indirect aerosol impacts on climate) of IPCC-2001 Report.³⁵

A number of monographs^{1–4} published in late seventies – early eighties had summarized previous works to study the aerosol effect on climate. More recently, some results obtained within CAENEX and GARREX observational field programs had been revised in the context of the problem of excess shortwave (SW) absorption.^{10–13} By the end of the twentieth century, three-dimensional global climate models have been developed, and they made it possible, in particular, to assess the potential climatic effect of aerosol in the situation, when attempts were undertaken to justify the concept of “global warming” due to emissions of greenhouse gases (primarily CO₂) to the atmosphere.

Since calculations assuming the gradual CO₂ growth (usually +1% a year) in the atmosphere had led to overestimation of atmospheric warming, a factor of

cooling due to purely scattering sulfate aerosol present in the atmosphere (or equivalent decrease of surface albedo) was introduced. Of course, it was merely a conditional procedure, and the results agreeing with observations were nothing more than fitting. Nevertheless, the problem of sulfate aerosol is undoubtedly important, so it is addressed in the first section of this review. Then, we discuss the existing estimates of climatic contributions of aerosols of other types (dust, carbon, biogenic, etc.). At last, much attention is paid to the problem of indirect influence of aerosol on climate, in particular, through the effect on cloud microstructure and optical properties.

1. Sulfate aerosol

Sulfate aerosol (SA) formed in gas-phase reactions from sulfur dioxide emitted to the atmosphere (primarily from burning of fossil fuels) plays an important role because of its abundance and purely scattering properties. Therefore, the SA-induced intensification of solar radiation backscattering to the outer space may be an important factor of atmospheric cooling. As was already mentioned above, taking into account only CO₂ growth and the associated greenhouse climate warming has led to overestimation of the globally mean annual surface air temperature (SAT), which motivated the importance of search for a cooling agent.

The supposition of the significant climatic role of sulfate aerosol is supported by the fact that SAT increase observed during past decades in the Southern Hemisphere (SH) was more significant than that in the Northern Hemisphere (NH) and the spatial SAT structure in the NH was far more complicated. This could be expected assuming an important contribution of sulfate aerosol to formation of the global SAT field.

As is well known, anthropogenic aerosol sources had intensified considerably during the past century. The sulfate aerosol is, possibly, the main component of the anthropogenic aerosol, though, of course, other aerosol types also cannot be ignored.³⁵ For the period from 1950 to present, industrial emissions of sulfur to the

atmosphere have doubled. The global budget of sulfur emissions is characterized by the data of Table 1 (Ref. 25).

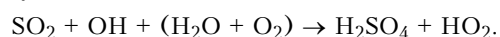
Table 1. Global budget of sulfur emissions, Tg (1Tg = 10¹² g)

Sulfur compounds	Emission sources	Level of emissions, Tg S/yr
Natural:		
DMS	Marine biosphere	18.1
DMS	Land biosphere	0.9
SO ₂	Volcanoes	8.0
Anthropogenic		
SO ₂	Biomass burning	2.5
SO ₂	Fuel and industrial fossil combustion	66.8
Total		96.3

As can be seen, the anthropogenic sources account for 72% of global sulfur emissions. Sulfates are the final product of a complex chain of physical and chemical processes causing conversion of gaseous sulfur compounds into solid matter, during which new particles are produced through either condensation (homogenous nucleation) or condensation on earlier existing particles. Anthropogenic emissions (making up to 80% of all sulfur emissions of non-sea origin) occur mainly in the form of sulfur gas.

However, it is important to remember that natural gaseous sulfur compounds (such as those associated with dimethylsulfide (DMS) and SO₂ emissions during volcanic eruptions) are transformed to sulfate aerosol (73%) more efficiently than anthropogenic compounds (58%), since the latter come to the atmosphere near the surface and are removed easier from the atmosphere by dry and moist deposition. About 50% of SO₂ are removed at the surface level by dry deposition and precipitation (moist deposition). Of the rest 50%, the least part is oxidized to gas-phase sulfate. At the same time, the most part of sulfate originates from heterogeneous chemical reactions in liquid phase in clouds. In this case, the oxidation rate depends not only on cloud parameters, but also on sulfate concentration, since its growth increases the acidity of cloud droplets and, hence, decreases the solubility of SO₂ as well as the rate of oxidation by ozone.

Recently, much attention has been paid to the study of gas-phase reactions of sulfate aerosol production because of its influence on formation of acid precipitation, impact on climate and, possibly, human health. In east Mediterranean region in summer, sulfate particles are largely produced in the reaction involving hydroxyl:



To study the dynamics of sulfate aerosol in the east part of the Mediterranean region, ground-based and airborne measurements of the concentration of sulfur dioxide and sulfate aerosol, as well as

measurements of meteorological parameters were performed at different Israel sites from time to time between 1984 and 1993.

Analysis of observations has revealed the higher concentration of sulfate aerosol than elsewhere in the world.^{49a} At some locations, the maximum aerosol concentration exceeded 500 nmol/m³ in summer; while in winter it ranged from 50 to 100 nmol/m³. The annual mean value was found to be (100 ± 15) nmol/m³, twice as large as that calculated for the studied region using the global model of sulfate aerosol formation and close to observations in the northeastern USA.

There are many features indicating that the sulfate aerosol has nonlocal origin and is carried to the studied region by long-range transport, namely, (1) the absence of correlation between the concentrations of aerosol and sulfur gas, (2) large concentration ratios of sulfate aerosol and total sulfate SO₄²⁻ / (SO₂ + SO₄²⁻) obtained from back trajectory calculation, and (3) the fact that close values of aerosol concentration were simultaneously observed in different geographic regions.

All the available observations suggest that the sulfate aerosol concentration reaches its diurnal maximum at afternoon hours, especially, in summer at inland sites. This diurnal behavior is not caused by long-range transport, but rather by the presence of seven significant sources of sulfur emissions to the atmosphere along Mediterranean coast of Israel.

The data of microstructure observations of non-sea-salt (NSS) sulfate aerosol in global marine atmospheric boundary layer (ABL) indicate that most particles of this aerosol have diameter > 1 μm, typical of sea-salt particles. These large particles typically have high rate of dry deposition, necessitating accounting for the influence of this process on sulfur balance in the marine ABL. Depending on observation conditions, the amount of such coarsely dispersed NSS aerosol may range from very small values to 5 nmol/m³ and higher.

Sievering et al.⁶⁸ have discussed the results of impactor observations made as a part of the first field Aerosol Characterization Experiment (ACE-1) at Cape Grim Baseline Air Pollution Station (CGBAPS) near north-western tip of Tasmania (Australia). They have found that, for the total concentration of NSS sulfate aerosol of 2.2–2.3 nmol/m³, this aerosol has the trimodal size distribution and the coarsely dispersed fraction of sea-salt aerosol (whose concentration is about 1 nmol/m³) with the particle diameter of 0.7 μm. Since the coarsely dispersed sea-salt aerosol was not related to ammonium, the cloud processing contributed only little to formation of the NSS fraction considered here, which, probably, originated from ozone-induced oxidation of SO₂ contained in sea-salt aerosol water (SSAW).

The realizability of this mechanism, however, depends strongly on the seawater alkalinity, which can be increased due to involvement of carbonates in the form of small fragments of biogenic CaCO₃ from the oceanic surface microlayer. However, even accounting for this factor, the oxidation of SO₂ contained in

SSAW can explain production of 70–90% NSS sulfates in sea-salt aerosols.

Since the sea-salt aerosol not subject to chemical processing can be responsible for about -2 W/m^2 change in the globally mean annual radiative forcing (RF), it seems necessary, in estimating the potential anthropogenic climate changes, to take properly into account modifications of properties of the sea-salt aerosol subject to processing. The change of the sulfur cycle in the marine ABL due to ozone-induced SO_2 oxidation in SSAW has another important aspect. Since most of dimethylsulfide (DMS) emitted to the atmosphere by marine organisms is converted into SO_2 in the marine ABL, the intensification of dry deposition of NSS aerosol and, correspondingly, removal of coarsely dispersed aerosol fraction from the marine ABL can lead to substantial change in the feedback between greenhouse warming, DMS emissions, and albedo of sulfate haze.

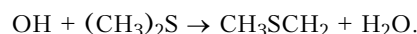
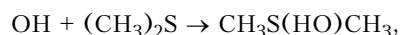
Many field measurements in different regions of the World Ocean and coastal zones indicate that DMS is the primary volatile sulfur compound coming to the atmosphere from ocean that is responsible for approximately 90% of biogenic emissions to the atmosphere. Therefore, DMS may play an important role in the global sulfur cycle; while the gaseous products of DMS oxidation (primarily SO_2 , $\text{CH}_3\text{S}_2\text{O}$, and H_2SO_4) may be components of gas-phase reactions of formation of cloud condensation nuclei (CCN) influencing the cloud microstructure and hence the albedo.

Dimethylsulfide is produced from biological activity of phytoplankton, and its production depends on a number of meteorological characteristics (primarily insolation). This last determines a feedback working such that the DMS-induced changes in clouds entail variations of the solar radiation incoming to the ocean and, thus, influence the dynamics of phytoplankton and the DMS emission rate. Although the existing estimates showed that the anthropogenic component dominates in total emissions of gaseous sulfur compounds to the atmosphere (primarily in the form of SO_2), the reliable determination of natural DMS emissions is of critical importance as well.

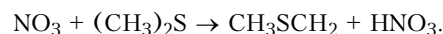
In this regard, in June 1992 Putaud and Nguyen⁵⁵ performed ship observations of dimethylsulfide concentration in seawater at three altitudes (1, 6, and 20 m) above the sea level to the south of Azores (34–37°N, 23–26°E) as a part of the Surface of Oceans: Fluxes and Interaction with the Atmosphere (SOFIA) Project. Simultaneously, meteorological and micrometeorological observations were carried out. The data on the ocean surface temperature, as well as the data on turbulent fluctuations of wind velocity and air temperature and humidity were used to calculate the coefficient of turbulent exchange between the atmosphere and ocean. The values of this coefficient were used to determine the DMS flow (emissions) from ocean to the atmosphere by means of different techniques.

Analysis of observations has shown that the vertical profiles of the DMS concentration in the 1–20 m layer under these conditions cannot be interpreted as being directly caused by vertical turbulent mixing (in view of the fact that the concentration frequently increased with height). Undoubtedly, in some cases a significant role was played by buoyancy preventing turbulence generation and by horizontal advection of air with the substantially different DMS concentration (especially at 20 m height). Only in four cases of 29, it has been possible to apply the gradient method of DMS flow calculation assuming that the flow keeps constant with height. Based on the earlier estimate, the globally mean DMS flow is $(0.48 \pm 0.33) \text{ Tmol/yr}$, or equivalently $(15 \pm 10) \text{ Tg S/yr}$. With regard for the results discussed here, the estimate of 0.53–0.67 Tmol/yr (17–21 Tg S/yr) should be considered most accurate to within $\pm 0.11\text{--}0.14 \text{ Tmol/yr}$ (3.5–4.5 Tg S/yr). We should keep in mind, however, that the gradient method calculates DMS flows with large error ($\pm 45\%$), and hence the obtained estimates are insufficiently reliable.

Despite the variety of mechanisms proposed to explain the processes of DMS oxidation and important for understanding the gas-phase formation of sulfate aerosol in the marine ABL, the problem of dimethylsulfide as a climate-forming agent is still far from solution. Most probably, the main mechanism of DMS oxidation is determined by DMS reactions with hydroxyl that possibly proceed in two ways:



The next reaction characterizes DMS oxidation caused by nitrate radical:



It is important to assess the role of each of these reactions and to determine the final products of DMS oxidation. James et al.³⁷ have performed a combined analysis (as a part of the Atmospheric Chemistry Studies in the Oceanic Environment (ACSOE) Project) of field observations and numerical experiments (based on a modified box model), which clearly demonstrated that the observed variations cannot be explained only by the daytime DMS oxidation rate by considering hydroxyl radicals only.

Reference 37 considers the observations in the framework of the quasi-Lagrangian scheme of field experiment at two sites of the eastern Atlantic Ocean (from a vessel and at Mace Head, 53°19'N, 9°54'W). The vessel was anchored so that the both observation sites were located on the path of the same air flow (thus, the observation data pertain to the same air "particle", but at different time). To check the validity of the above-mentioned model of chemical processes in the atmosphere, the measurements of the primary products of DMS oxidation (methanesulfonate MSA, sulfur gas SO_2 , and ions of non-sulfate aerosol SO_4^{2-})

were compared with the results of numerical simulation.

The main conclusion of Ref. 37 is that under the daytime conditions of marine air masses the model failed to predict the sufficient increase in the concentration of DMS oxidation products during the period of air transport from one site to another despite the overestimated rates of chemical reactions involving nitrogen in the process of advection and the agreement obtained between independent estimates of hydroxyl concentration in the course of measurements. Therefore, it was hypothesized that intensification of DMS oxidation in the marine ABL in daytime was caused either by halogen compounds (most probably, by halogen oxides BrO and IO), or by heterogeneous oxidation processes. Model calculations quite closely reproduce observation data if the 3.3 times larger rate of OH + DMS reaction is used (to compensate for neglect of other mechanisms of DMS oxidation). Measurements of the BrO and IO concentration gave, however, the insufficiently high values to produce such a strong intensification of DMS oxidation process, possibly because of the influence of an additional important factor, namely, reactions involving DMS in the liquid water phase.

The CLAW hypothesis suggests that the dimethylsulfide emitted to the atmosphere from the ocean is subsequently transformed in gas-phase reactions to submicron aerosol, whose particles can act as CCN and thus influence the cloud properties and climate. However, despite wide recognition, this hypothesis got in recent years, it still requires further justification. Sciare et al.⁶⁴ undertook analysis of the data of continuous ten-year (1990–1999) observations of the DMS concentration in the atmosphere at Amsterdam Island in the southern Indian Ocean (57°50'S, 77°30'E). This analysis has revealed a distinct annual behavior of the DMS concentration with twenty-fold variations of the amplitude from its maximum in January (i.e., during SH summer) to minimum in August (winter) as the concentration varied from 5 to 1930 pptv. It also revealed substantial deviations from the 10-year monthly mean values reaching 100% and probably explainable by the influence of meteorological conditions and/or oxidizing capacity of the atmosphere. Comparison of observations with numerical simulation results obtained using three-dimensional model accounting for chemical reactions and transport has demonstrated that the observed interannual variability can be explained assuming up to twice as large variations of the intensity of DMS sources. It was also shown that the variations of the DMS concentration correlate well with anomalies of the sea surface temperature, thus indicating the existence of correlation between DMS variations and climate.

It is important that sulfate particles are effectively washed out by cloud water and removed by precipitation. The production rate of sulfate aerosol

particles depends on such factors as the solar radiation, concentration of atmospheric gaseous components, and meteorological parameters (cloud amount, cloud liquid water content, and chemical composition of water droplets). In view of complexity of relevant chemical models, the earlier estimates of sulfate production rate substantially disagree. For this reason, the calculated vertical profiles of sulfate distribution differ considerably, despite the fact that near-surface concentrations are close in value. Validation of the obtained results is very difficult because no vertical profile observations (except ground-based measurements) are available.

Because of the important role of sulfate aerosol, the global sulfur cycle, undoubtedly, has attracted great attention in recent years. Estimates pertaining to the globally mean situation suggest that now about 70% of emissions of sulfur compounds to the atmosphere have anthropogenic origin, with only about 30% left for natural emissions. Although the scarce existing observations suggest, in particular, that land biogenic sources of emissions make relatively weak contribution, we still cannot explain geographic features of the distribution of different gaseous sulfur (especially biogenic) compounds on a regional scale. There are still no comparable data concerning the role of continental and marine biogenic sulfur sources, though, as is well known, shallow lakes and wetlands can contribute significantly to atmospheric emission of sulfur compounds.

In this regard, regular (daily) observations of methanesulfonate (MSA) concentration have been started in the central part of Canada, as well as on its Atlantic and Pacific coasts, supported by network observations of non-sea-salt sulfates (NSS SO_4^{2-}) and sulfur dioxide gas (SO_2). Li et al.⁴⁸ have considered the results of first-year (from April 1992 to June 1993) observations, primarily concentrating on analysis of the annual behavior. The observations made on the Atlantic coast (New Scotland, 44°22'N, 65°12'W) showed that the concentrations of the above-mentioned compounds varied in the ranges <0.002–0.13, 0.2–26, and <0.2–10 $\mu\text{g}/\text{m}^3$ with the mean annual values of 0.02, 2.2, and 1.3 $\mu\text{g}/\text{m}^3$.

The annual MSA behavior is characterized by the presence of a maximum at 0.036 $\mu\text{g}/\text{m}^3$ in June; whereas the maximum of the SO_2 concentration (2.7 $\mu\text{g}/\text{m}^2$) was observed in February, and for NSS SO_4^{2-} no distinct annual behavior was observed. The ratio of the MSA to the NSS SO_4^{2-} concentration was found to be less than elsewhere in the world, while the dominating factor of the annual behavior of this ratio was found to be variation of the methanesulfonate concentration. In the central part of Canada (49°31'N, 93°43'W) the concentration of the studied compounds was shown to be lower than on the coast and ranging as <0.002–0.066, 0.04–12.5, and <0.16–16.6 $\mu\text{g}/\text{m}^3$ with the mean annual values of 0.01, 1.6, and 0.93 $\mu\text{g}/\text{m}^3$. The annual behavior had maxima in September

(0.01 $\mu\text{g}/\text{m}^3$ for MSA), in March (2.1 $\mu\text{g}/\text{m}^3$ for NSS SO_4^{2-}), and in January (2.8 $\mu\text{g}/\text{m}^3$ for SO_2). The concentration ratio MSA/NSS SO_4^{2-} was close to that for the Atlantic coast. On the Saturn Island (British Columbia, 48°47'N, 123°08'W), the concentration variability ranges were 0.002–0.2 for MSA, 0.14–6.4 for NSS SO_4^{2-} , and 0.12–21 $\mu\text{g}/\text{m}^3$ for SO_2 with the mean annual values of 0.06, 1.1, and 3.0 $\mu\text{g}/\text{m}^3$, respectively. The observed concentrations reached maxima (0.12 $\mu\text{g}/\text{m}^3$) in August for MSA, (5 $\mu\text{g}/\text{m}^3$) in February for SO_2 , and (nominally, 1.5 $\mu\text{g}/\text{m}^3$) in August for NSS SO_4^{2-} . The annual behavior of MSA/NSS- SO_4^{2-} was dominated by MSA variations and characterized by the presence of maximum (0.1) in August.

It is well recognized now that the chemical processes in clouds influence considerably the global sulfur cycle, primarily, through cloud processing of aerosols, which leads to substantial change of aerosol properties (in particular, aerosol microstructure). Earlier studies have demonstrated how much this processing contributes to the growth of the intensity of light scattering by aerosol particles and to the increase of aerosol activity as cloud condensation nuclei (CCN) at low supersaturation. The latter process can lead to a change in the cloud microstructure, because cloud droplets are produced on cloud-processed aerosol particles.

Thus, a sort of feedback is formed that determines the interaction between aerosol and cloud particles. Numerical simulation of sulfate particle formation in clouds with allowance for cloud microstructure has shown that sea-salt particles not only affect sulfate formation, but also strongly modulate the increase of CCN activity and efficiency of aerosol scattering under the conditions of aerosol processing by marine clouds. In addition, the observations demonstrated that sulfate formation in non-activated sea-salt particles of marine haze can influence substantially the sulfur budget in the marine ABL. This process can likely have an important effect on the scattering efficiency and CCN activity, as in clouds.

To check if it is true, Hegg et al.³¹ performed comparative numerical simulation, whose analysis has shown that intensification of sulfate formation takes place in both clouds and non-activated haze, but only in clouds this has a significant influence on scattering and CCN formation. Table 2 illustrates the calculated variations of sulfate concentration $\Delta[\text{SO}_4]$, aerosol optical depth $\Delta\tau$, and CCN (ΔCCN) for four scenarios of aerosol processing by clouds and haze over sea for background and polluting (anthropogenic) aerosol. (Relative variations in % are given in parentheses; *RH* is relative humidity; *t* is the period of calculations.)

The obtained results show that for 8 h a large portion of SO_2 (19 and 146 pptv, respectively) has been converted to sulfate in the both haze cases, and in the case of background aerosol important factors were

not only SO_2 oxidation, but also non-marine (NSS) sulfate, whose concentration has doubled. The influence on scattering, however, was found to be insignificant.

Table 2. Aerosol processing by clouds and haze

Scenario	$\Delta[\text{SO}_4]$, pptv	$\Delta\tau$	ΔCCN
Marine background haze aerosol, 93% <i>RH</i> , <i>t</i> = 8 h	0.08	0.0001(1)	0.1 (1)
Marine anthropogenic haze aerosol, 93% <i>RH</i> , <i>t</i> = 8 h	0.62	0.003 (4)	6 (0.6)
Marine background cloud aerosol, <i>t</i> = 0.5 h	0.36	0.0009 (11)	57 (511)
Marine anthropogenic cloud aerosol, <i>t</i> = 0.5 h	2.96	0.023 (34)	13 (1.5)

Quite a different situation occurs for clouds under conditions favoring formation of aerosol particles optically active in the visible spectral region. A significant specificity was revealed from comparison of the data on variations of CCN concentration.

In addition to the direct effect on the radiation balance (through increase of solar radiation backscattering), SA also has an important indirect effect by contributing to the process of cloud formation and to cloud properties. In this regard, it is highly important to take interactively into account the processes of atmospheric thermohydrodynamics and cloud formation, as well as chemical processes (in particular, through modeling the interaction between sulfate aerosol and clouds, which causes the increase of cloud albedo due to sulfate aerosol).

Feichter et al.²⁵ first performed such an integrated simulation using Max Planck Institute for Meteorology (Hamburg University) ECHAM4 GCM. The important features of the model's radiation parameterization include incorporation of different greenhouse gases (such as water vapor, CO_2 , methane, nitrous oxide, and 16 chlorofluorocarbons) and aerosol types, as well as water vapor continuum absorption. The amount of clouds is approximated as a function of relative humidity.

Overall, the main features of calculated spatiotemporal variations of cloud liquid water content (LWC) well correspond to satellite data, but the discrepancy in the globally mean (regional) LWC achieves 1.5 (2.0) times (the calculations, in particular, fail to reproduce neither the contrast between subtropical and middle latitudes, nor the summer maximum of LWC in subtropical oceans of the Eastern Hemisphere). The model calculations overestimate SW CRF throughout a year in the regions of active convection over the tropical ocean and underestimate it over ocean in midlatitude summer.

The global sulfur cycle is simulated numerically using three model-predicted sulfur species (Table 2): two gases, namely, dimethylsulfide (DMS) and sulfur dioxide (SO_2), as well as sulfate aerosol (SO_4^{2-}). The advective transport of these components and their

vertical mixing in ABL are described similarly to the case of water vapor. The DMS and SO₂ oxidation during a day due to reactions with hydroxyl is considered. In addition, DMS is allowed to react with nitrate radicals (NO₃) at night. It is assumed that the only final product of DMS oxidation is SO₂. The final product of reactions of both gas- and liquid-phase SO₂ oxidation is considered to be sulfate SO₄²⁻. The calculated sulfate concentration serves as input data for calculation of aerosol radiative forcing (the scenario of current sulfur emissions is determined by the data of Table 1).

To estimate the direct and indirect climatic effects of sulfate aerosol, Feichter et al.²⁵ performed three types of experiments (first two covering the period of five years with “speed-up” time of three months): (1) EXP1, taking into account present sulfur emissions; (2) EXP2, assuming preindustrial conditions (i.e., total global emission rate of 27.2 Tg/yr). The difference in the SW radiation fluxes calculated taking into account the total aerosol (including variable sulfate aerosol) and using only the models of standard aerosol of other types is defined as sulfate aerosol radiative forcing. The difference EXP1 – EXP2 characterizes anthropogenic contribution to radiative forcing; and (3) EXP3 was aimed to estimate the errors due to using the average (monthly mean) distribution of sulfate aerosol in the case of EXP1 (the calculations were made for one-year period and three-month “speed-up” time). The optical properties of sulfate aerosol were calculated for particles of a 75% solution of sulfuric acid (density of 1.7 g/cm³) characterized by the lognormal microstructure with the modal radius of 0.07 μm.

On the globally average basis, about 50% of the mass of sulfate aerosol resides below the 800 hPa level; whereas in the Northern Hemisphere the 900 hPa (1 km) – 700 hPa (3 km) layer holds approximately 80% of sulfate mass. The data of Tables 3 and 4 characterize the average values of direct and indirect RF. As can be seen, the globally mean annual value of direct RF due to anthropogenic aerosol is –0.35 W/m². The annual behavior has a maximum in August and a minimum in December. The total RF is –0.57 (on the global scale), –0.79 (NH), and –0.35 W/m² (SH).

Calculations of the geographic distribution of direct RF have revealed the presence of the absolute maximum (–3 W/m²) in July in eastern United States and over Central Europe. Over the SH ocean, the radiative forcing ranges from 0 to –0.2 W/m². The indirect radiative forcing reaches the absolute maximum (–5 W/m²) in January over Pacific near the Asian coast, over Southern Africa, as well as near coasts of Peru and Brasilia. The globally mean value (due to aerosol-driven cloud albedo variations) is –0.76 W/m² (Table 3).

Of key importance is the significant difference in the geographic distributions of direct and indirect radiative forcing, with the former being maximal over polluted continental regions and the latter being larger

over ocean than over land. Table 3 illustrates this situation, in analysis of which it should however be remembered that the computation error is much larger for the indirect RF than for the direct one.

Table 3. The globally and hemispherically mean RF, W/m²

RF	EXP2 (preindustrial aerosol)	EXP1–EXP2 (anthropogenic aerosol)	EXP1 (present aerosol)
Direct			
annual mean,			
global	–0.23	–0.35	–0.57
NH	–0.24	–0.55	–0.79
SH	–0.22	–0.13	–0.35
Direct monthly			
mean,			
January, NH	–0.22	–0.40	–0.62
July, SH	–0.24	–0.79	–1.03
Indirect			
annual mean,			
global			
NH	–	–0.76	–
SH	–	–1.04	–
Indirect			
monthly mean,			
January, NH	–	–0.46	–
July, SH	–	–0.68	–
July, SH	–	–1.42	–

Table 4. Annual mean direct and indirect RF (W/m²), and total content of continental and oceanic sulfate (SO₄²⁻, mg/m²) due to anthropogenic emissions

Region	Direct		Indirect		Total sulfate content	
	Land	Ocean	Land	Ocean	Land	Ocean
NH	–0.64	–0.51	–0.83	–1.19	5.01	2.79
SH	–0.19	–0.12	–0.37	–0.49	1.59	0.75

The growth of the indirect RF over ocean is explained by the fact that marine clouds have lower number concentration of cloud droplets and so, they are more subject to the aerosol effect. Simulations have shown that if the monthly mean sulfate concentration is used for calculations, they overestimate substantially (by as much as 20% in the case of globally mean values and 100% on a regional scale) the indirect RF and leave the direct RF almost undisturbed. Feichter et al.²⁵ assert that numerical simulations should be aimed at account for differences in the spatial distributions of the direct and indirect RF using interactive description of chemical and meteorological processes, taking into consideration real variety of atmospheric aerosol.

Taylor and Penner⁷⁰ performed numerical simulation of climate using the interactive National Center for Atmospheric Research (NCAR) Community Climate Model (CCM1) version 1 of the atmosphere/ocean system coupled with the Lawrence Livermore National Laboratory (LLNL) model of chemical processes in the troposphere, which describes the gas-phase reactions (involving hydroxyl OH) of formation of sulfate aerosol from dimethylsulfide and sulfur gas and transport of sulfate aerosol in the atmosphere (GRANTOUR model).

The calculations showed that the CCM1 model well replicates the real climate, despite some underestimation of the surface air temperature primarily due to substantial systematic errors in the upper troposphere (Table 5). A good agreement exists between the observed and calculated values of the Earth Radiation Budget (ERB) components, but the annual behavior of cloud radiative forcing (CRF) is underestimated. When specifying sulfur gas emissions, industrial sources and fossil fuel/biomass burning are taken into consideration. Total emissions, approximately corresponding to the level of 1980, are assumed to be 78 Mt S/yr.

The numerical climate modeling covering the period of 20 years was performed using four scenarios: (1) preindustrial conditions (with CO₂ mixing ratio of 275 ppmv); (2) present CO₂ concentration (345 ppmv); (3) combination of present anthropogenic emissions of sulfur species (at the level of 1980) and CO₂ with concentration of 275 ppmv; and (4) the same as in the case 3, but with the CO₂ concentration of 345 ppmv. The data of Table 5 are calculations averaged for the last decade.

As can be seen, the globally mean values of radiative forcing signify a weak net climate warming effect (of course, it is important to remember that the calculations disregard the indirect aerosol effect on cloud optical properties, contributing significantly to ERB variations).

Analysis of the data on the geographic RF distribution, as well as on the CO₂ and aerosol contributions to climate change has shown that the maximum of aerosol-induced cooling is located over

vast NH continental regions, but not concentrated in the region of RF maximum over Europe, because the aerosol effect comes as a complex interplay with the mechanisms of atmospheric general circulation (and, in particular, variations of ice conditions in the Norwegian and Greenland Seas are of great importance).

Interestingly, when CO₂ and aerosol effects are taken into account simultaneously, the analysis reveals no RF increase in NH high latitudes; this increase is typical of greenhouse climate warming. Another feature is that the greenhouse and aerosol effects on climate are not additive: the linear model predicts global warming exceeding the considered warming by approximately 40%. The sensitivity of the used climate model determined by the ratio of the globally mean T_s and RF values was found to be very high (6.4°C for doubled CO₂ concentration); so Taylor et al.⁷⁰ emphasized the need in subsequent analysis of model adequacy. The presence of characteristic regional structures in the field temperature in response to anthropogenic forcing necessitates the search for corresponding signatures for identifying corresponding perturbations.

Using the atmospheric general circulation model (GCM) developed at the Hadley Centre for Climate Prediction and Research (United Kingdom), Jones et al.³⁸ estimated the geographic distribution of annual mean variations of radiation balance in the surface/atmosphere system (RBS) due to indirect effect of anthropogenic sulfate aerosol. The addressed effect is considered as a consequence of variations of optical parameters of low-level clouds under the effect of cloud condensation nuclei (CCN) produced in gas-phase nucleation reactions involving sulfur gas.

Table 5. Radiative forcing (RF) and corresponding climate change

Cases	RF, W/m ²	T _s , °C	ΔT _s , °C	P, mm/day	ΔP, mm/day	C, %	ΔC, %	SI, %	ΔSI, %
<i>Preindustrial level</i>									
Northern Hemisphere		12.5		3.40		56.6		4.87	
Southern Hemisphere		12.5		3.54		62.4		6.64	
Global		12.5		3.47		59.5		5.76	
<i>Present CO₂ concentration</i>									
Northern Hemisphere	1.26	14.5	1.9	3.48	0.09	55.0	-1.7	4.13	-0.74
Southern Hemisphere	1.25	14.8	2.3	3.61	0.08	61.1	-1.3	4.39	-2.26
Global	1.26	14.6	2.1	3.55	0.08	58.0	-1.5	4.26	-1.50
<i>Present sulfate concentration</i>									
Northern Hemisphere	-1.60	11.3	-1.2	3.36	-0.04	56.9	0.3	5.54	0.67
Southern Hemisphere	-0.30	11.7	-0.8	3.48	-0.06	63.1	0.7	7.24	0.59
Global	-0.95	11.5	-1.0	3.42	-0.05	60.0	0.5	6.39	0.63
<i>Combined effect of CO₂ and sulfates</i>									
Northern Hemisphere	-0.34	13.0	0.5	3.43	0.03	55.8	-0.9	4.85	-0.02
Southern Hemisphere	0.95	13.6	1.1	3.56	0.02	62.1	-0.3	5.40	-1.24
Global	0.31	13.3	0.8	3.49	0.02	58.9	-0.6	5.13	-0.63
<i>Observed values</i>									
Northern Hemisphere		14.9		2.6		58.9		4.4	
Southern Hemisphere		13.5		2.7		65.6		4.5	
Global		14.2		2.7		62.2		4.5	

Notes. T_s is surface air temperature, P is precipitation rate, C is cloud amount, SI is relative size of ice cover.

The used GCM includes a cloud prognostics module pre-computing the cloud ice and liquid water, as well as parameterization of the effective radius of water cloud droplets for different cloud types, CCN concentrations, and cloud liquid water contents. The two-stream approximation for SW radiation transfer describes the dependence of the cloud radiative properties on the cloud LWC and the effective radius of cloud droplets.

It is assumed that clouds contain only liquid water at the temperature above 0°C and only ice water at the temperature below -15°C, provided that continuous transition from one cloud type to another exists. Random cloud overlap in the vertical direction is considered. The aerosol is assumed to consist of sulfate ammonium and to have the lognormal particle size spectrum with the median radius of 0.05 μm. The vertical aerosol profile is such that the half of aerosol mass is concentrated in the lower 1.5-km layer of the atmosphere. The annual aerosol concentration ranges from less than 100 cm⁻³ over remote oceanic regions to more than 800 cm⁻³ over Central Europe. The number concentrations of cloud droplets N_{tot} and aerosol A are related by the following equation:

$$N_{tot} = 375[1 - \exp(-2.5 \cdot 10^{-3} \cdot A)].$$

The effective radius is defined by the equation

$$r_e = (3L / 4\pi\rho k N_{tot})^{1/3},$$

where L is cloud LWC, ρ is water density, and the parameter k is equal to 0.80 for marine clouds and 0.67 for continental clouds. The mean r_e values were found to be 1.3 μm larger over ocean than over land and 2.4 μm larger in the Southern Hemisphere than in the Northern Hemisphere; they are in qualitative agreement with satellite data. The aerosol effect on climate was estimated (applying GCM mentioned above) accounting for either total or natural aerosol concentration (naturally, the difference between these estimates characterizes the contribution of anthropogenic aerosol, neglecting the effect of feedback mechanism).

The analysis of r_e calculations for low-level clouds in the Northern Hemisphere has revealed a decrease in the effective drop radius over the most part of the land, especially, in main industrial regions; this has led to RBS decline, i.e., to climate cooling due to the effect of anthropogenic aerosol on cloud optical properties. The maximum cooling was obtained for locations where r_e decrease was the largest and where lower-level clouds were not screened by overlying clouds.

The annual globally mean RBS decrease was found to be -1.26 W/m², half as small as the greenhouse warming to be reached by the present time. The corresponding values for the Northern and Southern Hemispheres are -1.54 and -0.97 W/m². Since the direct impact of anthropogenic aerosol on RBS was estimated to be from -0.3 to -0.9 W/m², it is clear that the mean values of greenhouse warming and aerosol cooling are very close.

However, it is important to remember that a considerable uncertainty exists in estimates of the aerosol effect on climate. For instance, these estimates completely ignore the contribution of non-sulfate aerosol, as well as the influence of variable cloud microstructure on cloud evolution and precipitation formation. It is also important to take into account the sensitivity of clouds to variations of aerosol concentration and properties that is the highest in the case of clouds formed in clean marine air masses. This is especially true for SH oceanic regions, where, even for the moderate level of anthropogenic aerosol disturbance, the corresponding climatic consequences can be considerable (this increased sensitivity could be especially appreciable at the first stage of industrial revolution). Possibly, in the future this sensitivity will become weaker, leading to the less appreciable indirect influence of aerosol on climate.

One of the important features of long-term variations of the surface air temperature (SAT) is their asymmetry with respect to day and night time. Analysis of SAT observations in different regions of the world has shown that the most marked variation is the increase of the nighttime minimal temperature accompanied by the increase of cloud amount and the decrease of the amplitude of diurnal temperature variations. Analogous variations (considerable increase of the minimal SAT level and decrease of the amplitude of diurnal behavior) were revealed in numerical climate modeling which assumed the increasing CO₂ concentration in the atmosphere.

An anomalous situation was observed in India, where a warming trend (similar to the global and hemispherical trends) was accompanied by the growth of the amplitude of diurnal SAT variations. In some Indian regions, a relatively stable level of minimal SAT values was detected. The previous calculations have shown that these features can be explained if the local negative radiative forcing due to sulfate aerosol over Indian subcontinent is considered in combination with the global greenhouse effect. Besides, the results of numerical simulation are sensitive to parameterization of physical processes determining the amplitude of diurnal temperature variations, such as water cycle, cloud formation, and processes over land surface.

Lol et al.⁴⁹ undertook numerical simulation of the influence of sulfate aerosol on extremes of the surface air temperature in the Indian subcontinent using the interactive model developed at Deutsches Klimarechenzentrum (DKRZ), Hamburg, for the atmosphere/ocean system. Earlier calculations made using the same model and taking simultaneously into account the growth of greenhouse gases and the SA forcing are in a good agreement with SAT observations on the Indian territory over last 100 years.

The new calculated data on regional variations of extreme SAT values in 1980–1989 are in a good agreement with observations. The prognostic estimates obtained for the decade of 2040 (in comparison with

1980) show that the mean annual maximal and minimal SAT values increase by 0.7 and 1.0°C, respectively, with the most pronounced growth of the maximal (minimal) temperature observed in the monsoon (post-monsoon) period. Over land areas of the Indian subcontinent, the amplitude of diurnal variations substantially decreases in winter; however, it remains almost unchanged in the monsoon period. Analysis of the results of numerical simulation indicates that the main factors influencing the reliability of the results are the horizontal resolution and parameterization of physical processes. Lol, Srinivasan, and Cubash⁴⁹ underscore that in the future it is necessary to study the indirect aerosol effect on cloud radiative properties and, hence, cloud radiative forcing.

As was noted by Satheesh and Ramanathan,⁶³ from December to April of every year, the atmosphere/ocean system functions in the regime most suitable to perform field experiment to observe aerosol radiative forcing. Trace gas constituents and polluting aerosol components emitted to the atmosphere all over the northern part of the Indian subcontinent and the southern Asian region suffer long-range transport over the northern Indian Ocean due to the presence of stable north-eastern monsoon flow and reach tropical latitudes up to 5–10°N.

To study such a situation, Satheesh and Ramanathan⁶³ have undertaken a complex field Indian Ocean Experiment (INDOEX) to analyze the influence of anthropogenic aerosol on climate and chemical processes in the atmosphere. This experiment initiated in 1996 and reaching the intensive operations period (IOP) in January–March 1999 was based on shipborne, satellite-borne, and ground-based observations. In particular, at a specially created Kashido Climatic Observatory (KCO) (4.965°N, 73.466°E) located approximately 500 km south-west of the Indian subcontinent, continuous measurements of microphysical, chemical, and radiative aerosol properties were performed starting from February 1998.

Measurements of the aerosol optical depth (AOD) at the wavelength of 0.5 μm gave the values in the range from 0.2 to 0.7 for the following contributions of different aerosol types: 29% (sulfates and ammonium), 17% (sea salt and nitrate), 15% (mineral dust), 11% (soot), 20% (organics), and 8% (ash). The single scattering albedo for the entire set of aerosol types varied from 0.87 to 0.9. The anthropogenic sources contributed about 60% or more to AOD. In the period of winter monsoon, air masses from India or South Asia dominated in the KCO region (for about 90% of time).

In addition to KCO observations, simultaneous data on the ERB components (accurate to within 0.2%) were also available from the NASA Clouds and the Earth's Radiant Energy System (CERES) satellite for studying ERB and cloud cover. All the data were also used to validate the aerosol-radiative atmospheric model. Satheesh and Ramanathan⁶³ compare this model with the observed radiative forcing. In winter, the atmosphere in this region of the tropical Indian Ocean

in Northern Hemisphere is characterized by the high content of different types of anthropogenic aerosol (sulfate, nitrate, organic, soot, and ash) arriving from the Asian continent. Just this caused the decrease of SW RF in the range of 12–30 W/m² under clear skies at the surface level during winters of 1998 and 1999, whereas at the top of the atmosphere (TOA) this decrease was only 4–10 W/m². Such a discrepancy of the RF values at the surface level indicates that aerosol in the tropical atmosphere can substantially slow down the water cycle. An important fact following from analysis of ice cores drilled in Western Europe is that after 1850 the concentration of black carbon has increased by a factor of three.

A special emphasis was given to the study of anthropogenic sulfate aerosol (SA) (in view of the evidence that the SA concentration tends to increase in the atmosphere due to the growing human activity⁶¹). It was shown that, for a fixed cloud LWC, the cloud optical depth increases proportionally to $N_d^{1/3}$, and, on the other hand, aerosol limits formation of cloud droplets capable of fall as rain, since the decrease of water droplet size and number concentration leads to slowing down of the processes of drop collision and coalescence.

As was already noted above, the aerosol radiative forcing occurring through modification of cloud optical properties is conventionally called the indirect effect. Just this, still poorly understood, factor is characterized by most uncertain estimates of aerosol radiative forcing, which can be the reason for negative radiative forcing counterbalancing the greenhouse warming.

Rotstayn⁶¹ obtained new estimates of indirect aerosol climate forcing using Commonwealth Scientific and Industrial Research Organization (CSIRO) 18-level spectral global climate model (GCM) run on about 3.2°×5.6° latitude-longitude grid. An important feature of this model is the use of a detailed (in a physically based manner) parameterization scheme of cloud formation that takes into account the indirect anthropogenic aerosol forcing occurring through the change of the drop number concentration and cloud microstructure, as well as the lifetime of nonprecipitating clouds.

The N_d variations are specified from the data concerning N_d dependence on the monthly mean sulfate concentration, whose spatial distribution is calculated using the global GRANTOUR model of sulfate transport taking into account chemical processes. In this model, the anthropogenic sources of sulfur species are SO₂ emissions due to fossil fuel and biomass burning. The natural sources are biogenic emissions by ocean (DMS), soil (DMS, H₂S), vegetation cover (H₂S), and volcanoes (H₂S, SO₂). The influence of anthropogenically induced N_d variations is accounted for in precipitation calculations (this allows estimating the effect of SA-induced variations and the lifetime of nonprecipitating clouds) and the effective radius of

cloud droplets r_e (required to calculate SW and LW radiation transfer).

The r_e values calculated for the current conditions agree well with the r_e values retrieved from satellite data of cloud radiance measurements; though the model results underestimate somewhat the observed land/ocean and interhemispheric contrasts. The globally mean total indirect aerosol radiative forcing was estimated to be -2.1 W/m^2 , including the LW RF found to be $+0.1 \text{ W/m}^2$ (seemingly, this value is underestimated somewhat). The SA effect on clouds shows itself in the increase of the cloud amount by 1%, cloud liquid water by 6%, and the decrease of the effective droplet radius by 7%.

The special numerical experiments have demonstrated that variations of the total indirect radiative forcing due to variations in r_e and cloud lifetime are, respectively, -1.2 and -1 W/m^2 . The calculated results indicate that the radiative forcing also depends on the relationship between sulfate emissions and N_d , on the vertical SA distribution, and some other factors. However, in each of these cases, the RF caused by variations of the lifetime of nonprecipitating clouds is no less than 25% of the total RF, suggesting the importance of accounting for this factor in estimates of the indirect influence of anthropogenic aerosol on climate.

Since the submicron particles of sulfate and other types of anthropogenic aerosol can serve as CCN, as was already mentioned above, a possible consequence of aerosol influence on liquid water clouds can be an increase in the drop number concentration N_d . The previous experiments with the use of general circulation models (GCMs) have estimated the influence of the increasing cloud optical depth caused by the N_d increase, as an indirect influence of anthropogenic aerosol on cloud optical properties and climate. There is, however, another possibility of indirect influence associated with suppression of precipitation due to N_d growth. Analysis of this effect did not receive due attention so far, even though the reduction of precipitation due to anthropogenically induced growth of N_d is known from observations for already more than 30 years.

Using an 18-level spectral GCM at low (R21) horizontal resolution, Rotstajn et al.⁶² performed calculations in order to estimate the indirect influence of anthropogenic aerosol keeping in mind the two effects mentioned above. The used interactive model of the atmosphere/ocean system (taking into account the oceanic mixing layer) provides for realistic parameterization of stratus cloud dynamics, as well as realistic consideration of cloud-radiation interaction. The most important feature of the counterbalancing response of precipitation to anthropogenic aerosol forcing is the southward shift of equatorial precipitation zone, presumably due to the heat asymmetry between the Northern and Southern Hemispheres at the decrease of the sea surface temperature (SST).

This conjecture is justified by two numerical experiments performed using different SST fields: an observed SST in one experiment and the NH SST increased by 1 K in the other to simulate the preindustrial conditions. The first experiment, in comparison to the second one, gives the southward shifted equatorial precipitation zone, similarly to the effect of anthropogenic aerosol. The used GCM predicts the globally mean increase of the surface air temperature by 3.6 K in response to CO_2 doubling, whereas cooling due to aerosol is 2.9 K (corresponding to radiative forcing of -2.6 W/m^2).

In context of the study of different climatic factors, the interest to analysis of the effect of atmospheric aerosol and minor gases on cloud microphysical processes (and, in particular, the role of decrease of water vapor pressure over water droplets due to surface-active species²⁴) has increased considerably in recent years. In particular, an attention was paid to the influence of such minor gases as gaseous nitrogen acid and ammonium, acting to activate cloud condensation nuclei (CCN). In this regard, in development of analogous study performed earlier, Hegg³² undertook numerical simulation of the influence of NH_3 and HNO_3 uptake by aerosol particles on CCN activation.

The typical microstructure of atmospheric aerosol is characterized by the presence of the submicron acid component (accumulation mode) and the coarsely dispersed alkali mode (sea-salt aerosol over ocean and alkali dust aerosol on land). The HNO_3 uptake is caused primarily by particles of coarsely dispersed alkali aerosol and, since such particles initially have quite large size to act as CCN, the influence of HNO_3 uptake can be only minimal as a factor of CCN number concentration. Therefore, it is especially important to analyze the influence of NH_3 on acid aerosol particles.

Calculations made for moderately polluted continental clouds and relatively clean marine stratocumulus clouds have shown that, in clouds over sea, the microphysical processes can modify strongly due to NH_3 uptake by particles, so that cloud microstructure and, hence, cloud albedo can substantially change. The results of numerical simulation indicate that the influence of uptake of minor gases by aerosol particles on cloud albedo is comparable to that due to strong variations of the number concentration of coarsely dispersed aerosol particles. This suggests that our understanding of the mechanisms of indirect aerosol effect (through modification of cloud optical and microphysical properties) on climate need serious revision.

In numerical climate simulation, the single scattering albedo is usually used as an optical parameter that describes radiation scattering and absorption by aerosol; whereas the amount of aerosol in the atmosphere is preset by specifying aerosol emissions taking into account the level of fossil fuel burning. This approach involves a number of assumptions producing (not quantified yet) overestimation of the aerosol radiative forcing.

Rond and Charlson⁶⁰ have suggested a new approach to determining the radiative forcing. It is based on the use of *in situ* measurements to account for aerosol absorption. For this, they introduced the absorption cross section Q_{abs} calculated per unit time (m^2/s), which can be directly used in diffusion and transport models for pre-calculation of the three-dimensional nonstationary distribution of aerosol absorption in the visible spectral region. It is given as $Q_{\text{abs}} = Q_f EF_{\text{pm}} F_{\text{fine}} F_{\text{abs}} \alpha_{\text{abs}}$, where Q_f is the amount of burned fuel; EF_{pm} is the emission coefficient (the amount of aerosol calculated per unit mass of burned fuel); F_{fine} is the number of particles with the diameter less than $1 \mu\text{m}$ (larger particles more rapidly fall out, so they are not taken into account); and F_{abs} is the fraction of aerosol particles absorbing radiation; α_{abs} is absorption coefficient.

The product of the first four terms gives the emission level of absorbing aerosol (primarily elemental carbon). Global emissions were estimated to range from 1.9 to 8.3 Tg/yr.

Langmann et al.⁴⁶ estimated the climatic effect of sulfate aerosol (SA) taking into account the inhomogeneity of the global distribution of SA precursor gases (produced in gas-phase reactions) on the basis of the combined use of the Hamburg Institute (Max Planck Institute for Meteorology) Regional Atmospheric model (HIRAM) and the improved EURAD chemistry-transport model. This model allows simulation of not only direct variations of SW radiative forcing (RF) due to sulfate aerosol, but also the indirect influence on RF through SA-induced variations of cloud microphysical and optical properties.

The data of Langmann et al.⁴⁶ suggest that the cloud amount substantially influences climate and, therefore, the cloud dynamics must be carefully taken into account to estimate correctly both direct and (especially) indirect SA effect on climate. One of the interesting conclusions is that about one third (33% in summer and 56% in winter) of the SA contribution to RF over European continent comes from the natural SA (dimethylsulfide and volcanic aerosol). The long-range transport of primary and secondary atmospheric pollutants also is an important climate-forming agent.

In recent years, different hypotheses have been put forward to explain possible mechanisms of global climate stabilization by means of a feedback caused by biogenic aerosol. For instance, Shaw^{66,67} justified a mechanism, according to which the biogenic sulfate aerosol particles may lead to the growth of the albedo of the atmosphere/surface system and, correspondingly, to climate cooling which compensates for the increase of the sea surface temperature and the associated growth of dimethylsulfide emissions by the ocean.

These (and other similar) hypotheses of climatic stability are based on the assumption of the active participation of biota showing itself as the increase of DMS emissions in the course of SST growth or decrease of solar radiation, as well as on the presence of the

positive correlation between the increasing DMS emissions and the increasing sulfate aerosol concentration (total concentration or just CCN concentration). However, these hypotheses are not reliably supported by observations. Ramanathan and Collins suggested an alternative thermostat mechanism, not involving the assumption on biogenic sulfate aerosol and based on the fact that SST never rises above 302 K. Based on this, it was concluded that cirrus clouds formed in the upper part of the penetrative convection system have a regulating effect on the tropical climate.

Shaw et al.⁶⁷ tried to justify a new hypothesis claiming that the climate stabilizing feedback acts due to biogenic sulfur "pumped" by penetrative convection into the intertropical convergence zone from the marine atmospheric boundary layer (ABL) to the middle and upper troposphere. Aerosol particles formed from sulfur species in the free troposphere then sink to the marine ABL, where they influence the process of cloud formation by acting as CCN, whose presence favors the growth of the cloud droplet concentration. The associated increase of the cloud albedo leads to the decrease of the solar radiation available for absorption by the ocean and, hence, to the decrease of SST.

For such a scenario, the discussed feedback is as follows: SST increase \rightarrow convection intensification \rightarrow CCN concentration growth \rightarrow increase of cloud droplet concentration and cloud albedo \rightarrow reduction of the solar radiation available for absorption by ocean \rightarrow SST decrease \rightarrow weakening of convection, etc. Two important features of the conjectured scenario are the following: (1) feedback intensity is controlled by convective transport of biogenic sulfur to the upper troposphere (rather than the increase of sulfur emissions by ocean at global warming, i.e., an active role of marine biota, that was hypothesized earlier) and (2) cooling near the ocean surface is caused by the increase of the cloud albedo in the marine ABL due to intensification of convectively driven sulfur transport. Since low-level clouds do not influence the greenhouse effect, the albedo effect of clouds is unambiguous. Of course, the mechanism outlined above needs in further verification against observation data.

2. Aerosol radiative climate forcing

To characterize the climatic effect of the atmospheric aerosol, calculations of aerosol radiative forcing are most frequently used. Haywood and Shine²⁸ calculated the direct aerosol effect when using the spectral algorithm developed by Edwards and Slingo (two-stream delta-Eddington approximation) for calculation of shortwave radiative fluxes taking into account 24 spectral intervals (this allowed them to treat quite adequately the absorption by water vapor, carbon dioxide, and ozone, as well as Rayleigh scattering). The aerosol radiative forcing is determined as the difference between the values of shortwave

radiation balance at TOA level calculated with and without allowance for the aerosol effect.

Numerical simulation was performed for clear-sky and cloudy conditions with inclusion of sulfate and soot aerosol for different values of the surface albedo (from 0 to 1), solar zenith angle, and relative humidity. The microstructure of sulfate aerosol (SUA) is specified by a lognormal distribution. It is assumed that sulfate aerosol consists of ammonium sulfate particles with radii of 0.05 μm under dry conditions (with dispersion of 2.0) and soot aerosol (SOA) particles with radii of 0.0118 μm (dispersion of 2.0). The extinction coefficient for sulfate (soot) aerosol at the wavelength of 0.55 μm is 5.0 (9.3 m^2/g). The single scattering albedo for sulfate aerosol is specified by the Lagrener-Rodhe model, while its total column content is taken to be 3.2 mgSO_4/m^2 to give the optical depth of 0.016 at the wavelength of 0.55 μm . When specifying the spatial variability of SUA and SOA, the constant SOA/SUA ratio is assumed. The ratio of SOA mass concentration (due to fossil fuel burning) to anthropogenic SUA is set to $M_{c/\text{SO}_4} = 0.075$, corresponding to the soot aerosol optical depth of 0.0022 (with mentioned arbitrariness of all the specified values).

Calculations have shown that SOA radiative forcing is maximal over surfaces with low albedo for the solar zenith angle no larger than 70°. Due to the influence of relative humidity, the SOA effect on radiative forcing is stronger if SOA is located at lower altitudes in the atmosphere. For albedo in excess of 0.5, small positive values of radiative forcing take place. Estimates of aerosol longwave forcing have shown that it is positive for both SUA and SOA, but an order of magnitude (or more) lower than the shortwave radiative forcing.

Analysis of the obtained results has demonstrated that in future treatments of direct radiative forcing within climate models it is necessary to take into account subgrid-scale variations of relative humidity, as well as the spatial correlation between clouds and regions of increased relative humidity. The earlier parameterization of the direct SUA effect on climate assuming the equivalent change of surface albedo overestimates radiative forcing by a factor of 2–3 (in comparison with the multispectral calculations mentioned above).

The cloudy atmosphere contributes negligibly to direct radiative forcing in the case of SUA, but has a considerable (RF enhancing) effect if the SOA resides inside or above the clouds. An important finding of numerical simulation of the direct aerosol effect on climate is that the presence of even small amount (compared with sulfate aerosol) of soot may lead to considerable positive radiative forcing (especially in the case of high surface albedo), so that aerosol will have the warming rather than cooling effect on climate. Therefore, adequate specification of the vertical profile of the soot concentration relative to the cloud layer is very important. Undoubtedly, complex field experiments are urgently required to obtain realistic input parameters for adequate numerical simulation.

Using refined models of sulfate and carbon aerosol, Haywood and Ramaswamy²⁹ have obtained new estimates of the contribution of these aerosol types to the global distribution of radiative forcing. For calculation of (SW only) radiative forcing, the R30 climate model developed in the Geophysical Fluid Dynamics Laboratory (GFDL) at the Princeton University (USA) was used. This model employs radiation parameterization based on the two-stream delta-Eddington approximation (assuming the lognormal aerosol size distribution for preset values of the complex refractive index).

The calculations have shown that for sulfate aerosol (SA) the single scattering albedo is almost equal to unity over the entire shortwave spectral range, whereas for carbon aerosol (CA) it is lower than 0.35 and strongly decreasing with wavelength. In the both cases, the extinction coefficient decreases so rapidly with the increasing wavelength and has so small values in the IR spectral region that insignificance of radiative forcing due to thermal infrared radiative transfer can be concluded.

The radiative forcing is calculated as a difference of the SW radiation balance of the atmosphere/surface system obtained with and without allowance for aerosol when specifying the mean solar zenith angle for calculation of monthly and annual mean radiative forcing (the numerical simulation is performed for the period of one year using the preset annual SST behavior). The annual mean radiative forcing due to sulfate aerosol was found to be $-0.8 \text{ W}/\text{m}^2$ (respectively, -1.40 and $-0.24 \text{ W}/\text{m}^2$), whereas the value recommended by the IPCC-95 Report is $-0.40 \text{ W}/\text{m}^2$ determined accurate to a constant factor of 2.

Since the discrepancy between calculated values of radiative forcing is caused by quite many factors, the contributions of individual factors can hardly be estimated. The globally mean radiative forcing due to carbon aerosol is approximately $+1.1 \text{ W}/\text{m}^2$, but, for a number of reasons, the more realistic value is $+0.4 \text{ W}/\text{m}^2$ determined accurate to a constant factor of 3. Since the data on the microstructure and on the submicron fraction of carbon aerosol are still highly uncertain, it is reasonable to use normalized (to unit aerosol mass) radiative forcing in the range from $+1.1$ to $+1.9 \text{ W}/\text{m}^2$ ($-0.46 \text{ W}/\text{m}^2$ for SA).

The global distribution of normalized radiative forcing due to both sulfate and carbon aerosol is characterized by very strong spatial inhomogeneity. For reliable RF determination, it is important to have data on the vertical profiles of sulfate and carbon aerosol. Estimates have shown that the contribution of sulfate aerosol to radiative forcing is the most significant in lower atmospheric layers, where the SA dependence on the relative humidity is most evident, while the contribution of carbon aerosol (CA) is the strongest in the lower troposphere (above clouds). Hence, reliable calculations of transport of different aerosol types (taking into account the aerosol chemical transformation) and, correspondingly, the three-

dimensional aerosol distribution in the global atmosphere (in particular, taking into account aircraft effluents of CA) are required.

Given the globally mean radiative forcing of -0.8 for SA and $+0.4 \text{ W/m}^2$ for CA, the net radiative forcing will be -0.4 W/m^2 , assuming that the two aerosols form an external mixture (if, however, the aerosols are internally mixed, then the radiative forcing would be more positive). It should also be remembered that the real atmospheric aerosol is much more diverse. The neglect of this circumstance, as well as the absence of quite reliable data on the abundance of different aerosol types, specific features of vertical profiles, influence of the moisture content, and optical characteristics of real aerosol explain the still high uncertainty of calculated radiative forcing.

According to the available estimates, the climate sensitivity parameter (the sensitivity of globally mean annual surface air temperature to variations of radiative forcing) is $(0.65 \pm 0.26) \text{ K}\cdot\text{m}^2/\text{W}$, suggesting that RF variations on the order of a few W/m^2 should produce substantial climate changes. As is well known, the radiative forcing due to the growth of greenhouse gases (such as CO_2 , CH_4 , N_2O , and CFC_s) has been approximately equal to 2.5 W/m^2 since 1800. Therefore, quite reliable estimate of aerosol RF is of great importance. In this regard, Pan et al.⁵⁰ undertook analysis of possible uncertainties in the estimates of direct RF due to sulfate aerosol, whose shortwave component was calculated to range from 0.28 to 1.3 W/m^2 .

The purpose of this analysis is to obtain a combined estimate of RF uncertainty due to errors in the input parameters (in contrast to the sensitivity to changes of individual parameters). This parametric uncertainty can be characterized either by the probability density function (PDF) or by the average value and the confidence interval for a studied variable when specifying possible variability of the input parameters. The structural differences are determined by the differences between mean values for all considered models. The comparison of parametric uncertainty and structural difference can serve to justify the priority of the input parameters.

To determine the parametric uncertainty, a computationally efficient second-order probability collocation method (PCM) was used together with four different structural aerosol models and 13 input

parameters (with a preset probable variability). The main attention was paid to analysis of structural (model) differences due to varied optical aerosol properties (such as extinction, single scattering albedo, and asymmetry parameter of the scattering phase function) and radiative transfer computation error.

To calculate the globally mean diurnal radiative forcing due to anthropogenic SA throughout the atmospheric depth, four box models were used taking into account: (1) the observed optical aerosol properties (OAP) at the wavelength of $0.55 \mu\text{m}$ (D1); (2) the roughly calculated OAP dependence (for a given microstructure) on the wavelength (D2); and (3, 4) more accurately calculated OAP spectral dependences (D3, D4). In the D1 model, the OAP values are approximated using the observed values at the wavelength of $0.55 \mu\text{m}$. In the D2–D4 cases, the OAP spectral dependences are calculated at 24 wavelengths (in the wavelength range of $0.3\text{--}4 \mu\text{m}$) for the aerosol microstructure and the particle refractive index specified by taking into account the dependence of the specific extinction coefficient ψ_e on the relative humidity RH : $\psi_e(\lambda, RH) = \psi_e(\lambda) f_{RH}$. Radiative fluxes were calculated by the doubling method (D1, D2) and using more perfect methods (D3, D4).

The data of Table 6 characterize the values of 13 input parameters and their possible variations (uncertainty factor). Ten listed parameters are used in D1 and nine are used in D2–D4 models. For all of the parameters (except for r_g , σ_g , RH , and H), a lognormal distribution about a central value is assumed. The sulfate aerosol microstructure is also characterized by the lognormal distribution, in which the accumulation mode particles predominate. Variations of the relative humidity are described by the β -distribution with the mean value of 75% and the variance of 13%. The probability density function of the aerosol layer depth has the associated mean value $H = 1.5 \text{ km}$ with the variance of 1.5 km .

The comparison of the calculated results has shown that PDFs for RF corresponding to the D2–D4 models agree fairly well. However, the D1 model, which neglects the spectral AOP dependence, considerably overestimates the mean RF and the corresponding variance. An important finding is that the data obtained using the PCM method and those obtained with the computationally expensive Monte Carlo method (MCM) agree (10000 tests versus 55 representative PCM runs).

Table 6. Central values and uncertainty factors of input parameters

Parameter	Q , 10^{12} g S/yr	Y	t , day	r_g , μm	σ_g	ψ_e , m^2/g	β	$1 - R_s$	$1 - A_c$	T	f_{RH}	RH	H , km
Model	D1–D4	D1–D4	D1–D4	D2–D4	D2–D4	D1	D1	D1–D4	D1–D4	D1–D2	D1	D2–D4	D2–D4
Central value	71.0	0.5	5.5	0.0488	2.00	5.0	0.3	0.85	0.39	1.76	0.39	β -	1.42
Uncertainty factor	1.15	1.5	1.5	1.26	1.16	1.4	1.3	1.1	1.2	1.2	1.2	distribution	1.4

Notes. Q is the sulfur emission rate (10^{12} g S/yr); Y is the fraction of emitted sulfur gas transformed to sulfate aerosol; t is aerosol lifetime (days); r_g and s_g are mean geometrical particle radius (μm) and its variance; β is the fraction of backscattered radiation; R_s is surface albedo; A_c is cloud amount; T is transmission of the mixed aerosol layer; H is the aerosol layer thickness.

Table 7. Mean values, variance, and 95% confidence intervals of radiative forcing due to anthropogenic sulfate aerosol (W/m^2)

Model	Mean value		Variance		Confidence interval	
	MCM	PCM	MCM	PCM	MCM	PCM
D1	1.2	1.3	1.0	1.0	0.4–4.2	0.1–4.0
D2	0.41	0.43	0.35	0.33	0.1–1.4	1.1–1.3
D3	0.28	0.28	0.20	0.18	0.1–0.78	1.1–0.71
D4	0.35	0.37	0.25	0.25	0.1–0.99	0.1–1.0

Table 7 presents the calculated mean values, variance, and 95% confidence intervals for RF due to anthropogenic aerosol. As can be seen, the parametric nonuniformity is within the range of 0.1–4.2 W/m^2 at the 95% confidence level, whereas the estimated sensitivity (structural differences) mentioned above lies in the range of 0.28–1.3 W/m^2 . Excluding the D1 model, these ranges decrease down to 0.28–0.43 W/m^2 , i.e., become much less than the parametric uncertainty. Hence, to decrease the uncertainty level of estimates, it is primarily necessary to obtain adequate values of input parameters rather than to refine the model structure.

Aside from uncertainty estimates, the PDF analysis allows one to rank different factors according to their contribution to the total variability under influence of different uncertainties. This analysis has led to the conclusion that the largest contributions for the D1 model are made by Y , t , T , ψ_e , RH , and β . For all the other models, ranking of the contributions is the same except for the R_s contribution in the D3–D4 cases, substantially exceeding the R_s contributions in the D2 and D4 models. As can be seen, the largest contributions come from the uncertainty in sulfur emissions, aerosol lifetime, and relative humidity (interestingly, the contribution of particle size has appeared to be small, suggesting that it is sufficient to specify reliably the aerosol mass concentration). As to the model sensitivity to 1% uncertainty in the input parameters, the increase of all the input parameters (except for σ_g and R_s) entails the increase of RF because RF is negative. The D1 model is most sensitive to β , A_c , T , and t variations, whereas all the other models are sensitive to r_g , A_c , and R_s variations. Pan et al.⁵⁰ underscored the tentative character of these estimates, because of the specific choice of models and the uncertainty characteristics of input parameters, as well as the possible correlation between individual parameters.

Very active recent debate of the anthropogenic impact on the global climate was concentrated primarily at estimates of anthropogenically induced variations of radiative forcing (RF) due to the growth of carbon dioxide (and other greenhouse gases) leading to climate warming, as well as climate cooling due to sulfate aerosol (a number of papers point out to the necessity of considering the real diversity of aerosol types and, correspondingly, accounting for aerosol absorption of shortwave radiation).

Sinha and Harries⁶⁹ noted that climate characteristics may change even for the zero net

globally mean RF not leading to changes in the globally mean surface air temperature, despite zero local RF due to CO_2 and aerosol. To justify this, Sinha and Harries⁶⁹ performed calculations of the globally mean SAT using the one-dimensional radiative-convective atmospheric model, which assumes, in particular, the presence of low-, middle-, and high-level clouds with 26, 18, and 20% cloud fraction, respectively. Assuming the tropospheric temperature lapse rate of -6.5 K/km, the equilibrium SAT will be 286.7 K. Passage to the conditions of the perturbed atmosphere assumed doubling of the CO_2 concentration (from 355 to 710 ppmv) and addition of aerosol.

Since the globally representative aerosol data are absent, it was assumed (taking into account the aerosol radar sensing data) that one third of aerosol is concentrated in the upper troposphere (5–10 km), whereas the total content varied so as to reach the same equilibrium globally mean SAT (286.7 K) as typical of the unperturbed conditions. The corresponding atmospheric column aerosol content was 15.4 mg/m^2 , approximately four times higher than the current sulfate aerosol content in the atmosphere. In this case, the net RF due to CO_2 and aerosol is zero, because of mutual compensation (± 3.1 W/m^2). However, the vertical profiles of radiative temperature variations (radiative heat influxes) corresponding to the two equilibrium atmospheric states (perturbed and unperturbed) appear to differ substantially. Overall, the radiative cooling increases in the upper troposphere and decreases in the lower troposphere (with SAT remaining the same).

Though, understandably, the one-dimensional model cannot adequately describe the influence of the atmospheric dynamics, it is nevertheless clear that the static stability decreases under the conditions of the perturbed atmosphere. This should influence the formation of convection, precipitation, and other large-scale processes because of redistribution of heat influxes due to radiation and convection. Analogous estimates pertaining to RF balancing due to the increase in the CO_2 content and cloudiness (with varied characteristics) showed that the obtained results differ from those pertaining to aerosol. Thus, under conditions of zero net RF, different vertical profiles of heat influx can take place.

To assess the situation, in which both the global and local RF values are zero, Sinha and Harries⁶⁹ calculated average meridional profiles of radiative balance (RB) at the tropopause and surface levels, as well as the radiative heat influx to the atmospheric

depth for the unperturbed atmosphere and conditions with the doubled CO₂ concentration and aerosol addition in January and July. In this case, the July RF was comparable with the unperturbed January RF. Therefore, the aerosol content in each 10° latitude belt varies in such a way that the aerosol cooling in July corresponds to the local warming in January and, thus, the mean annual RF in each latitude belt (taken as an average of July and January values) is zero.

However, despite this, the values of the radiative balance at the surface and tropopause levels for the unperturbed atmosphere were found to differ from those for the CO₂ + aerosol atmosphere. These differences are large at the tropopause level, except for very high latitudes of the Northern Hemisphere where cooling in July ranges from 1 to -2 W/m², whereas warming of the same value takes place in the Southern Hemisphere (the January meridional profile is, by definition, a mirror image of the July profile). At the surface level, the maximum summertime (wintertime) cooling of -4 W/m² (-6 W/m²) takes place in the Northern (Southern) Hemisphere.

Thus, the radiative heat influx (radiation balance) for atmospheric depth is positive, reaching a maximum of about +4 W/m² at low latitudes. The meridional profile of the RF difference for the unperturbed and CO₂ + aerosol atmospheres is characterized by warming (for doubled CO₂ and addition of aerosol), reaching a maximum in the latitude belt ±35° (relative variation is about 3%) in the presence of symmetry about the equator (excluding near-polar regions, since heating near the north pole is much stronger than that in the region of the south pole).

Naturally, the atmospheric heating should lead to weakening of convection with associated consequences for precipitation. Since sustaining of invariable RF (even for the doubled CO₂ concentration) requires substantial reduction of solar radiation income due to aerosol, this also should influence photochemical processes and, thereby, lead to further climate change. Reduction of the solar radiation incoming to the surface will also influence the biospheric and cryospheric processes. In summer, the reduction of (both SW and LW) radiation budget will be 3–5 W/m², while in January it will reach -6 W/m² at the 35°S latitude (but increase up to positive values near the poles). The results considered here clearly show that RF cannot be used as a single factor determining climate change.

Conclusion

Summarizing, it is useful to discuss briefly the results of works within the International Global Atmospheric Chemistry (IGAC) Sub-Project of the International Geospheric Biospheric Program (IGBP) targeting atmospheric chemistry, aerosol, and climate as addressed in Ref. 18. Brasseur, the Chairman of IGAC, in his introductory paper correctly notes that one of the main uncertainties of numerical climate simulation lies

in the difficulty to treat the direct and indirect effect of atmospheric aerosol on climate. This difficulty is due to still poorly understood strong spatiotemporal variability of aerosol microstructure, multicomponent chemical composition, and optical properties.

As indicated by the results of numerous field observational experiments (ACE-1, ACE-2, ARM, KENEX, TARFOX, etc.), the local and even regionally mean values of aerosol radiative forcing (RF) can reach 20 W/m², far exceeding the globally mean aerosol RF (on the order of a few W/m²). Therefore, further serious effort is required to accumulate, on the basis of observations, the adequate information on aerosol on a global scale. This information will make it possible to estimate quite reliably the direct aerosol (including anthropogenic aerosol) influence on climate. Solution of this problem primarily requires observation data (including results of ground-based and satellite remote sensing). Nevertheless, no less important role is played by laboratory studies of aerosol properties and further development of numerical simulation of the aerosol effect on climate. It is even more difficult to take into account the indirect aerosol effect on climate through the influence of aerosol particles serving as cloud condensation nuclei (CCN) on cloud physical properties (especially cloud albedo) and chemical reactions in cloud droplets.

As noted by Fucchi, two families of liquid-phase substances, namely, sulfur species and organic compounds (the latter being most poorly understood), are key components of chemical reactions occurring in cloud droplets. An important aspect of the problem is the existence of the dependence between the chemical composition and the size of cloud droplets. For instance, inclusion of cloud microstructure yields a 3–4-fold increase in the S(IV)–S(VI) transformation rate. Another important aspect of the problem is that until recently the research in this field was focused only on the processes in warm liquid water clouds, whereas processes in cool ice water clouds remained almost totally beyond the scope.

In this regard, Hegg discussed in detail the problem of cloud–aerosol interaction. He analyzed the role of clouds and precipitation as aerosol sinks. Four interactive processes largely determine the cloud effect on aerosol: (1) vertical transport (especially true for convective clouds); (2) scavenging (both by water droplets and ice crystals) involving different mechanisms; (3) chemical processes in cloud droplets; and (4) formation of new aerosol particles in near-cloud environment.

For the scavenging process, the following features are most important: increase of the particle size range and decrease of the aerosol number concentration, development of a minimum in the size distribution (at least in the case of nonprecipitating clouds) for the particle size corresponding to effective supersaturation maximum (and the minimal activation radius). Most thoroughly studied chemical process is SO₂

transformation to sulfate in the liquid phase. The process of production of new particles near clouds is important because it is a significant CCN source.

Germann et al. have already analyzed possible ways of S(IV)–S(VI) transformation by considering clouds as regions of multiphase chemical transformation. The chemical composition of cloud droplets changes due to supply of water-soluble CCN components, as well as due to solution of trace gas constituents (TGCs) in cloud water. The calculations have shown that the S(IV) oxidation in tropospheric clouds on a global scale is 2–5 times more intense than outside clouds (though many details of this process need further study). The numerical simulation shows that the most intense oxidation is that involving hydrogen peroxide.

Facchini reviewed the problem of organic cloud chemistry and the influence of corresponding chemical processes on cloud properties. According to the initial conceptual model, cloud droplets contain an insoluble solid core surrounded by water solution of organic and inorganic components and covered by an organic surface film. This model characterizes droplets as complex heterogeneous systems; and the presence of organic components in them influences substantially the chemical and physical properties of droplets. This is especially true for photochemical reactions in liquid phase and for the processes on the droplet–atmosphere interface. The main water-soluble organic components (WSOC) include: formic, acetic, and other light carboxyl acids, formaldehyde and other carbonyl compounds formed from the gas phase, but water insoluble species are also important.

An important role is played by the aerosol WSOC components, such as the class of macromolecular polycarboxyl acids recently found in aerosol samples and having the properties similar to the characteristics of humic acids. Much attention is paid recently to studying the contribution of organic (especially surface-active) aerosol in CCN. The presence of many different classes of multiform organic species motivates radical change in our estimates concerning the role of chemical processes in clouds.

M. Bart discussed the problem of parameterization of the cloud effect on TGC in numerical models aimed to include the following three processes: (1) chemical processes inside and outside cloud droplets; (2) influence of aerosol on chemical processes in the liquid phase; and (3) cloud microphysics as an example of the influence of non-chemical processes on variations of the spatial distribution of chemical components.

K. Nun considered the problem of the indirect aerosol effect on climate, in particular, through change of cloud radiative characteristics (primarily cloud albedo) being one of the most acute aspects of climate research. In addition, it is necessary to take into account the influence of aerosol on the processes of precipitation formation and icing in mixed clouds. At last, aerosol can also influence the dynamic processes in

the atmosphere that are responsible for cloud formation and development. It is very important that the process ultimately determining the indirect aerosol effect on clouds and climate, namely, droplet or crystal growth occurs on timescales on the order of few seconds for characteristic spatial scales on the order of a few micrometers. At the same time, the final result of associated processes of cloud formation occurs on a global scale. Adequate description of the set of such processes is an extremely complicated problem, whose solution is possible only through collaboration between experimenters and numerical modelers.

The indicated results obtained within IGAC clearly illustrate the marginal complexity of the processes in the aerosol–clouds–climate chain. The following complex (focused) experimental and theoretical investigations should be accomplished (1) to improve our understanding of chemical and physical processes of formation, transformation, and transport of atmospheric aerosol (taking into account the anthropogenic effect) both in the clear-sky atmosphere and in the aerosol–clouds system; the obtained results should be used to validate aerosol models characterizing the global dispersion of aerosol properties; (2) to develop global climate models capable of reproducing realistically the aerosol effect on climate taking into account the real diversity of aerosol properties. In this regard, it is important to analyze the role and the possibility of allowance for interactive aspects of the problem, such as inclusion of sulfate aerosol (in interactive description of the global sulfur cycle) and cloud–aerosol interaction.

References

1. K.Ya. Kondratyev, *Modern Climate Change and Main Climate Forcing Factors*, Itogi Nauki i Tekhniki. Meteorologia i Climatologia (VINITI, Moscow, 1977), Vol. 4, 203 pp.
2. K.Ya. Kondratyev, *Radiative Factors of Modern Global Climate Change* (Gidrometeoizdat, Leningrad, 1980), 280 pp.
3. K.Ya. Kondratyev, *Stratosphere and Climate*, Itogi Nauki i Tekhniki. Meteorologia i Climatologia (VINITI, Moscow, 1981), Vol. 6, 223 pp.
4. K.Ya. Kondratyev, *Earth's Radiation Balance, Aerosol, and Clouds*, Itogi Nauki i Tekhniki. Meteorologia i Climatologia (VINITI, Moscow, 1983), Vol. 10, 315 pp.
5. K.Ya. Kondratyev, V.I. Binenko, V.F. Zhvaley, V.A. Ivanov, and N.E. Ter-Markaryants, *WMO Bulletin* **32**, No. 2, 132–139 (1983).
6. K.Ya. Kondratyev and N.I. Moskalenko, *Greenhouse Effect of the Atmosphere and Climate*, Itogi Nauki i Tekhniki. Meteorologia i Climatologia (VINITI, Moscow, 1984), Vol. 12, 264 pp.
7. K.Ya. Kondratyev, in: *Achievements in Hydrometeorology and Environmental Monitoring* (Gidrometeoizdat, Leningrad, 1987), pp. 57–97.
8. K.Ya. Kondratyev, *Atmos. Oceanic Opt.* **5**, No. 3, 208–211 (1992).
9. K.Ya. Kondratyev, *Atmos. Oceanic Opt.* **5**, No. 3, 212–222 (1992).

10. K.Ya. Kondratyev, V.I. Binenko, and I.N. Mel'nikova, *Meteorol. Gidrol.*, No. 3, 14–23 (1996).
11. K.Ya. Kondratyev, *Ecodynamics and Geopolitics*. Part 1: *Global Problems* (Publishing House of St. Petersburg Scientific Center of Russian Academy of Sciences, 1999), 1036 pp.
12. K.Ya. Kondratyev and V.I. Binenko, *Meteorol. Gidrol.*, No. 1, 33–41 (2000).
13. K.Ya. Kondratyev, K.S. Demirchan, S. Baluyas, V.I. Adamenko, S. Bommer-Kristiansen, Sh.B. Idso, D. Kukla, E.S. Postment'er, and V. Sun, *Global Climate Change: Conceptual Aspects* (NITsEB RAS, 2001), 125 pp.
14. K.Ya. Kondratyev and K.S. Demirchan, *RAS Bulletin*, No. 11, 1002–1009 (2001).
15. K.Ya. Kondratyev, *Atmos. Oceanic Opt.* **15**, No. 2, 105–124 (2002).
16. V.V. Penenko and L.I. Kurbatskaya, *Atmos. Oceanic Opt.* **11**, No. 6, 503–506 (1998).
17. V. Sun, S. Baluyas, K.S. Demirchan, K.Ya. Kondratyev, Sh.B. Idso, and E.S. Postment'er, *Izv. RGO* **133**, Issue 2, 1–19 (2001).
18. *Atmospheric Chemistry, Aerosols and Climate*. IGAC Activities Newsletter, No. 23 (2001), 23 pp.
19. C.P. Bahrman and V.K. Saxena, *J. Geophys. Res.* **D103**, No. 19, 25153–25161 (1998).
20. G. Brasseur and A. Pczenny, in *Global Atmospheric Chemistry*, IGAC Activities Newsletter, No. 46 (2001), pp. 7–9.
21. R.J. Charlson, J.H. Seinfeld, M. Kulmala, A. Laaksonen, and M.C. Facchini, *Science* **292**, 2025–2026 (2001).
- 21a. C.C. Chuang, J.E. Penner, K.E. Taylor, A.S. Grossman, and J.J. Walton, *J. Geophys. Res.* **102**, 3761–3778 (1997).
22. W.C. Conant, *J. Geophys. Res.* **D105**, No. 12, 15347–15360 (2000).
23. W.F. Cooke, C. Lioussse, H. Cachier, and J. Feichter, *J. Geophys. Res.* **D104**, No. 18, 22137–22162 (1999).
24. M.C. Facchini, M. Mircea, S. Fuzzi, and R.J. Charlson, *Nature* **401**, 257–259 (1999).
25. J. Feichter, U. Lohmann, and I. Schult, *Climate Dynamics* **13**, No. 4, 235–246 (1997).
26. A.B. Ghosh, S. Bose, M.C. Sharma, and B.S. Gera, *Indian J. Radio and Space Phys.* **29**, No. 1, 41–46 (2000).
27. J. Hansen, M. Sato, A. Lacis, and R. Ruedy, *Phil. Trans. R. Soc. London. B* **352**, 231–240 (1997).
28. J.M. Haywood and K. Shine, *Quart. J. Roy. Meteorol. Soc.* **123**, Part A, No. 543, 1907–1930 (1997).
29. J.M. Haywood and V. Ramaswamy, *J. Geophys. Res.* **D103**, No. 6, 6043–6058 (1998).
30. J. Haywood and O. Boucher, *Rev. Geophys.* **38**, No. 4, 513–543 (2000).
31. D.A. Hegg, R. Majled, P.F. Yuen, M.B. Baker, and T.V. Larson, *Geophys. Res. Lett.* **101**, No. 19, 2613–2616 (1996).
32. D.A. Hegg, *Geophys. Res. Lett.* **27**, No. 15, 2201–2204 (2000).
33. M. Hess, P. Koepke, and I. Schult, *Bull. Am. Meteorol. Soc.* **79**, No. 5, 831–844 (1998).
34. S.F. Iacobellis, R. Frouin, and R.C.J. Somerville, *J. Geophys. Res.* **D104**, No. 10, 12031–12045 (1999).
35. J.T. Houghton et al., eds., *IPCC, Climate Change 2001: The Scientific Basis* (Cambridge University Press, 2001), 881 pp.
36. M.Z. Jacobson, *Nature* **409**, 695–697 (2000).
37. J.D. James, R.M. Harrison, N.H. Savage, A.G. Allen, J.L. Grenfell, B.J. Allan, J.M.C. Plane, C.N. Hewett, B. Davison, and L. Robertson, *J. Geophys. Res.* **D105**, No. 21, 26379–26392 (2000).
38. A. Jones, D.L. Roberts, and A. Slingo, *Nature* **370**, 450–453 (1994).
39. J.T. Kiehl, T.L. Schneider, P.J. Rasch, M.C. Barth, and J. Wong, *J. Geophys. Res.* **D105**, No. 1, 1441–1458 (2000).
40. K.Ya. Kondratyev, *Radiation Processes in the Atmosphere*, WMO Monograph, No. 409 (Geneva, 1972), 214 pp.
41. K.Ya. Kondratyev, *Climate Shocks: Natural and Anthropogenic* (John Wiley & Sons, New York, 1988), 296 pp.
42. K.Ya. Kondratyev and I. Galindo, *Volcanic Activity and Climate* (A. Deepak Publ., Hampton, VA, 1997), 382 pp.
43. K.Ya. Kondratyev, *Multidimensional Global Change* (Wiley/PRAXIS, Chichester, U.K., 1998), 761 pp.
44. K.Ya. Kondratyev, V.I. Binenko, and I.N. Melnikova, *Meteorol. and Atmos. Physics* **65**, Nos. 1–2, 1–10 (1998).
45. K.Ya. Kondratyev, *Climatic Effects of Aerosols and Clouds* (Springer/PRAXIS, Chichester, U.K., 1999), 264 pp.
46. B. Langmann, M. Herzog, and H.F. Graf, *Atmos. Environ.* **32**, No. 16, 2757–2768 (1998).
47. J. Li, G.D. Wong, J.S. Dobbie, and P. Chylek, *J. Atmos. Sci.* **58**, No. 2, 193–209 (2001).
48. Sh.-M. Li and L.A. Barrie, *J. Geophys. Res.* **D101**, No. 2, 4165–4173 (1996).
- 48a. X. Li, S.A. Christopher, J. Chou, and R.M. Welch, *J. Appl. Meteorol.* **39**, No. 12, 2278–2291 (2000).
- 48b. C. Lioussse, J.E. Penner, C. Chuang, J.J. Walton, H. Eddleman, and H. Cachier, *J. Geophys. Res.* **101**, 19411–19432 (1996).
- 48c. U. Lohmann, J. Feichter, C.C. Chuang, and J.E. Penner, *J. Geophys. Res.* **104**, 24557–24563 (1999).
- 48d. U. Lohmann, J. Feichter, J. Penner, and R. Leitch, *J. Geophys. Res.* **105**, 12193–12206 (2000).
49. M. Lol, G. Srinivasan, and U. Cubash, *Curr. Sci. (India)* **71**, No. 10, 746–752 (1996).
- 49a. M. Luria, M. Peleg, G. Sharf, D.S. Tor-Alper, N. Spitz, Y. Ben Ami, Z. Gawii, B. Lifschitz, A. Yitzchaki, and I. Seter, *J. Geophys. Res.* **D101**, No. 20, 25917–25930 (1996).
50. W. Pan, M.A. Tatang, G.J. McRae, and R.G. Prinn, *J. Geophys. Res.* **102**, 21915–21924 (1997).
51. J.E. Penner, C.C. Chuang, and K. Grant, *Climate Dynamics* **14**, 839–851 (1998).
52. C. Pilinis and X. Li, *J. Geophys. Res.* **D103**, No. 4, 3789–3800 (1998).
53. M. Posfai, J.R. Anderson, P.R. Buseck, and H. Sievering, *J. Geophys. Res.* **D104**, No. 17, 21685–21694 (1999).
54. A. Pszenny, W. Keene, C. O'Dowd, M. Smith, and P. Quinn, *IGAC Activities Newsletter*, No. 11, 6–12 (1998).
55. J.-P. Putaud and B.C. Nguyen, *J. Geophys. Res.* **D101**, No. 2, 4403–4411 (1996).
56. Y. Qian and F. Giorgi, *J. Geophys. Res.* **D104**, No. 6, 6477–6500 (1999).
57. V. Ramanathan and K. Rajeev, *J. Geophys. Res.* (2001) (in print).
58. M.C. Reader and G.J. Boer, *Climate Dynamics* **14**, Nos. 7–8, 593–607 (1998).
59. H. Rodhe, *Nature* **401**, 223–225 (1999).
60. T.E. Rond and R.J. Charlson, *Geophys. Res. Lett.* **25**, No. 3, 337–340 (1998).
61. L.D. Rotstayn, *J. Geophys. Res.* **D104**, No. 8, 9369–9380 (1999).
62. L.D. Rotstayn, B.F. Ryan, and J.E. Penner, *Geophys. Res. Lett.* **27**, No. 19, 3045–3048 (2000).
63. S.K. Satheesh and V. Ramanathan, *Nature* **404**, No. 6782, 60–63 (2000).
64. J. Sciare, N. Mihalopoulos, and F.J. Dentener, *J. Geophys. Res.* **D105**, No. 21, 26369–26377 (2000).

65. J.H. Seinfeld and R.C. Flagan, IGAC Activities Newsletter, No. 17, 9–11 (1999).
66. G.E. Shaw, Atmos. Environ. **21**, 985–986 (1987).
67. G.E. Shaw, R.L. Benner, W. Cantrell, and A.D. Clarke, Clim. Change **39**, No. 1, 23–33 (1998).
68. H. Sievering, B. Lerner, J. Slavich, J. Anderson, M. Posfai, and J. Cainey, J. Geophys. Res. **D104**, No. 17, 21707–21718 (1999).
69. A. Sinha and J.E. Harries, Geophys. Res. Lett. **24**, No. 19, 2355–2358 (1997).
70. J.P. Taylor and J.E. Penner, Nature **369**, 734–737 (1994).
71. J.P. Taylor, M.D. Glew, J.A. Coakley, Jr., W.R. Tahik, S. Platnich, P.V. Hobbs, and R.J. Ferek, J. Atmos. Sci. **57**, 2656–2670 (2000).
72. I. Tegen, D. Koch, A.A. Lacis, and M. Sato, J. Geophys. Res. **D105**, No. 22, 26971–26990 (2000).
73. S. Twomey, Atmos. Environ. **A25**, 2435–2442 (1991).
74. M. Wendisch, J. Heintzenberg, and M. Bussemer, Meteorol. Zeitschr. **10**, No. 1, 45–60 (2001).
75. J.J. West, C. Pilinis, A. Nenes, and S.N. Pandis, Atmos. Environ. **32**, Nos. 14–15, 2531–2542 (1998).
76. M.A. Wetzel and L.L. Stowe, J. Geophys. Res. **D104**, No. 24, 31287–31300 (1999).
77. K. Wyser and J. Ström, Geophys. Res. Lett. **25**, No. 10, 1673–1676 (1998).
78. S. Yu, V.K. Saxena, B.N. Wenny, J.J. DeLuisi, G.K. Yue, and I.V. Petropavlovskikh, J. Geophys. Res. **D105**, No. 20, 24739–24750 (2000).